



HAL
open science

Active vibration control of a smart functionally graded piezoelectric material plate using an adaptive fuzzy controller strategy

Jonas Maruani, Isabelle Bruant, Laurent Gallimard, Frédéric Pablo

► To cite this version:

Jonas Maruani, Isabelle Bruant, Laurent Gallimard, Frédéric Pablo. Active vibration control of a smart functionally graded piezoelectric material plate using an adaptive fuzzy controller strategy. *Journal of Intelligent Material Systems and Structures*, 2019, 30 (14), pp.2065-2078. 10.1177/1045389X19853628 . hal-03019037

HAL Id: hal-03019037

<https://hal.parisnanterre.fr/hal-03019037>

Submitted on 23 Nov 2020

HAL is a multi-disciplinary open access archive for the deposit and dissemination of scientific research documents, whether they are published or not. The documents may come from teaching and research institutions in France or abroad, or from public or private research centers.

L'archive ouverte pluridisciplinaire **HAL**, est destinée au dépôt et à la diffusion de documents scientifiques de niveau recherche, publiés ou non, émanant des établissements d'enseignement et de recherche français ou étrangers, des laboratoires publics ou privés.

Active vibration control of a smart functionally graded piezoelectric material plate using an adaptive fuzzy controller strategy

Jonas Maruani, Isabelle Bruant , Frédéric Pablo and Laurent Gallimard

Abstract

In this article, the active vibration control of a smart structure made out of a single functionally graded piezoelectric material layer, equipped with a network of discrete electrodes, is studied. The material properties vary continuously across the direction of thickness, so that top and bottom surfaces consist of pure PZT4 and the mid surface is composed of pure aluminium. The percolation phenomenon is taken into account. A functionally graded piezoelectric material plate finite element based on the first-order shear deformation theory hypothesis and layer-wise approximation for electric potential is implemented. An optimization procedure is considered to define the relevant electrodes for actuators and sensors, based on controllable and observable criteria. An adaptive fuzzy controller system is used, activating with relevance the actuators according to the most excited eigenmodes. Simulations show the effectiveness of this kind of concept.

Keywords

Functionally graded piezoelectric material, active vibration control, finite element method, adaptive fuzzy controller

1. Introduction

In the recent years, a great deal of research on active vibration control in different domains of engineering has been carried out for light-weight smart structures using piezoelectric materials. Piezoelectric materials have been extensively used because they have specific characteristics, such as light weight and high strength. Moreover, they are easily shaped and have a good frequency response. These characteristics make them attractive actuators and sensors. The classical smart structures are multilayered composites with piezoelectric devices adhesively bound to the host structure, either at its surface or inside it (Preumont, 2011). These conventional smart structures suffer high stress concentration near interlayer surfaces because of abrupt changes in electro-mechanical properties. Moreover, the adhesive layer may crack at low temperatures and creep or peel at high temperatures (Pritchard et al., 2013), which can lead to severe deterioration of the interlayer bounding strength and performance response.

To overcome these shortcomings, the functionally graded piezoelectric material (FGPM), a new class of

the well-known functionally graded material (FGM) (Mahamood et al., 2012), has attracted much attention these last few years. They are designed to achieve a functional performance with mechanical and piezoelectric properties that gradually evolve along one or several directions. This continuity allows us to avoid the aforementioned disadvantages of classical piezoelectric smart structures. In this way, the substitution of a classical piezoelectric smart structure by a FGPM structure seems to be an attractive choice for active vibration control.

Most of available studies deal with the analysis of FGPM beams, but some others related to static and dynamic behaviour of FGPM plates can be found. These FGPM are usually made of a mixture of two piezoelectric materials. Among the published recent papers, static analyses have been performed in

LEME, Université Paris Nanterre, Ville d'Avray, France

Corresponding author:

Isabelle Bruant, LEME, Université Paris Nanterre, 50 rue de Sèvres,
92410 Ville d'Avray, France.
Email: isabelle.bruant@parisnanterre.fr

Brischetto and Carrera (2009), Behjat et al. (2011) and Nourmohammadi and Behjat (2016). Free vibration and dynamic response have been studied in Susheel et al. (2016), Behjat et al. (2011) and Barati and Zenkour (2018) who consider the effect of porosities.

Regarding the active vibration control using FGPs, many papers deal with active vibration control of FGM equipped with classical piezoelectric patch (often put all over the top and bottom faces of the structure). Restricting the bibliography to plate and shell structures, most of them use the classical velocity feedback gain control (He et al., 2001; Kiani et al., 2013; Sheng and Wang, 2009; Yiqi and Yiming, 2010). The displacement–velocity feedback control is performed by Liew et al. (2003), Zheng et al. (2009) and Fakhari and Ohadi (2011). Narayanan (2010) compares this kind of control with the H^2 control method. Narayanan (2010) considers the linear quadratic regulator to control the vibration of an FGM shell.

The active vibration control with FGPM is a relatively new topic and very limited works can be found in open literature. Non-linear active control of FG beams in thermal environments subjected to blast loads with integrated FGPM sensor and actuator layers (made by mixed two piezoelectric materials PZT4/PZT5H) was developed in Bodaghi et al. (2012). In Sharma et al. (2016) and Susheel et al. (2016), active vibration control of plates using PZT/Pt-based FGPM has been performed. In these three papers, sensors and actuators are made of FGPM and are bound symmetrically to the entire top and bottom faces of the host structure.

The present paper deals with active vibration control of an original smart structure. The usual host structure with several piezoelectric sensors and actuators is substituted by a single FGPM structure, which ensures continuity on the material properties. This FGPM is made of a mixture between PZT4 and aluminium, such that its composition varies symmetrically from aluminium at the mid surface to PZT4 at the top and bottom surfaces. Mixing dielectric and conductive materials leads to the percolation phenomenon: the FGPM switches from insulating behaviour to a conductive one according to the concentration of conductive particles (Chýlek and Srivastava, 1983; Pecharrómán and Moya, 2000). In order to activate piezoelectric properties for active vibration control, the FGPM's top and bottom faces are covered by a set of electrodes such as a printed wiring in electronics. These numerous configurations of electrodes then define the possible locations and dimensions of integrated sensors and actuators (collocated or not).

This smart conception overcomes the previous described drawbacks of active control with classical piezoelectric patches. In particular, the problem of patch release is avoided. A first study dealing with the active control of FGPM beams has been presented in

Maruani et al. (2017). Results show the effectiveness of this smart FGPM concept for 1D structure.

In this article, the active vibration control of thin plates is considered. In this case, the implementation of the control system is more complex: the actuator and sensor networks are bigger, the possible excitations are numerous. In order to insure a suitable active control whatever the external perturbations are, a smart adaptive controller has been developed. At each step of the active control process, according to the inputs of sensors, the control system defines the most excited eigenmodes and then uses the relevant actuators. The electric potential applied to the actuators is defined by a fuzzy logic controller.

The main originality of this study is the use of

- A smart structure made out of a *single* FGPM layer, having a network of discrete electrodes which allows to use some parts of the FGPM as sensors and actuators.
- Taking into account the percolation phenomenon in the FGPM plate model.
- An adaptative fuzzy controller system activating with relevance over time the actuators according to the most excited eigenmodes.

The present paper first presents the FGPM's behaviour laws using the volume fraction index k and the percolation threshold V_T . The finite element (FE) method is proposed to study the FGPM vibrations. The control system is detailed in the third section. Numerical results and discussion are conducted in the fourth and fifth section to show the efficiency of this new concept. The main conclusions are summarized in the last section.

2. FGPM plate model

We consider a plane and straight FGPM plate whose dimensions are the length L , the thickness h and the width b . The FGPM is made of a mixture of PZT4 and aluminium (Figure 1). We consider that the material properties vary continuously across the direction of thickness, so that top and bottom surfaces consist of pure PZT4 and the mid surface is composed of pure aluminium. It is supposed to be polarized along the z -axis.

2.1. Material behaviour laws

A mixture of dielectric and conductive components, respectively here PZT4 and aluminium, has particular electric properties when $V^{(m)}$ the concentration of the metallic component reaches the percolation threshold. At this concentration, noted V_T , the composite undergoes a conductive-insulator transition: below V_T , the

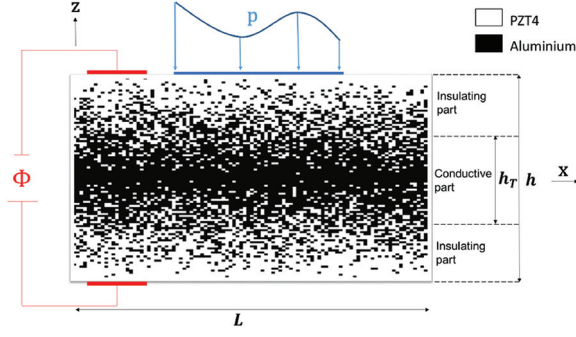


Figure 1. Schematic of the considered PZT4/Al/PZT4 FGPM.

composite has an insulating behaviour and above V_T , the composite has a conductive behaviour (Pecharrómán and Moya, 2000).

The percolation occurs when there are enough metallic particles to form a conductive path into the mixture. The percolation threshold is usually obtained through dedicated experimental measures and it depends on the micro-structure of the mixture (shape and size of materials' particles (Pecharrómán and Moya, 2000)). Based on models of percolation theory (Chýlek and Srivastava, 1983) and experimental studies (Li et al., 2001; Takagi et al., 2002), we shall assume that V_T varies in the range of 10%–30%.

Since the FGPM is assumed to be symmetrically distributed with respect to the aluminium mid surface, three regions can be identified: a conductive, aluminium-rich central region around the mid surface where the percolation has occurred and two outer insulating regions in which the concentration of metallic particles is below the percolation threshold (Figure 1).

2.1.1. Properties homogenization. The addition of metal particles into a dielectric matrix increases the composite's permittivity significantly. Effective medium theories such as the Maxwell-Garnett theory and the Bruggeman theory can be used to estimate the permittivity. In this study, particles are dispersed through a continuous ceramic matrix. The effective permittivity ϵ is thus given by the Maxwell-Garnett rule (Chýlek and Srivastava, 1983)

$$\epsilon(V^{(m)}) = \epsilon^{(p)} \frac{1 + 2V^{(m)} \frac{\epsilon^{(m)} - \epsilon^{(p)}}{\epsilon^{(m)} + 2\epsilon^{(p)}}}{1 - V^{(m)} \frac{\epsilon^{(m)} - \epsilon^{(p)}}{\epsilon^{(m)} + 2\epsilon^{(p)}}} \quad (1)$$

where $V^{(m)}$ is the metal volume fraction and p, m superscripts refer to piezoelectric ceramic and metal, respectively.

We assume that metal particles can be represented by a dielectric material with strong dielectric losses (i.e. with a dominant imaginary part), and the ceramic matrix can be represented by a perfect dielectric

material (without dielectric losses). In addition, at low frequencies, dielectric losses of metal particles tend to infinity. The effective permittivity constant becomes Li et al. (2001) and Orlowska (2003)

$$\epsilon(V^{(m)}) \simeq \epsilon^{(p)} \frac{1 + 2V^{(m)}}{1 - V^{(m)}} \quad , \quad \epsilon^{(m)} \gg \epsilon^{(p)} \quad (2)$$

A simple linear law of homogenization is used for other effective material properties P (elastic stiffness coefficients C_{ij} , density ρ) and can be expressed as Doroushi et al. (2011)

$$P = (P^{(m)} - P^{(p)})V^{(m)} + P^{(p)} \quad (3)$$

Poisson's ratio, ν , is considered constant in this study.

2.1.2. Power law distribution. We assume that the volume fraction varies according to a power law distribution along the z direction, which can be given as Doroushi et al. (2011)

$$V^{(m)}(z) = \left(1 - \frac{2|z|}{h}\right)^k \quad , \quad z \in \left[\frac{-h}{2}, \frac{h}{2}\right] \quad (4)$$

where k is the non-negative fraction index which may vary from 0 to ∞ .

The thickness of the conductive part h_T depends on both the percolation threshold and the fraction index and can be derived from equation (4) by setting $V^{(m)}(z = h_T/2) = V_T$

$$h_T = h \left(1 - V_T^{\frac{1}{k}}\right) \quad (5)$$

As a consequence, the piezoelectric constants e_{ij} are

$$e_{ij}(z) = \begin{cases} (e_{ij}^{(m)} - e_{ij}^{(p)}) \left(1 - \frac{2z}{h}\right)^k + e_{ij}^{(p)} & \frac{h_T}{2} \leq z \leq \frac{h}{2} \\ 0 & -\frac{h_T}{2} < z < \frac{h_T}{2} \\ (e_{ij}^{(m)} - e_{ij}^{(p)}) \left(1 + \frac{2z}{h}\right)^k + e_{ij}^{(p)} & -\frac{h}{2} \leq z \leq -\frac{h_T}{2} \end{cases} \quad (6)$$

Substituting equation (4) into equation (2), the effective permittivities are given by

$$\epsilon_{ii}(z) = \begin{cases} \epsilon_{ii}^{(p)} \frac{1 + 2\left(1 - \frac{2z}{h}\right)^k}{1 - \left(1 - \frac{2z}{h}\right)^k} & \frac{h_T}{2} \leq z \leq \frac{h}{2} \\ 0 & -\frac{h_T}{2} < z < \frac{h_T}{2} \\ \epsilon_{ii}^{(p)} \frac{1 + 2\left(1 + \frac{2z}{h}\right)^k}{1 - \left(1 + \frac{2z}{h}\right)^k} & -\frac{h}{2} \leq z \leq -\frac{h_T}{2} \end{cases} \quad (7)$$

The distribution in the direction of thickness of elastic stiffness coefficients C_{ij} , piezoelectric constants e_{ij} and effective permittivities ϵ_{ii} along the z direction is plotted in Figure 2.

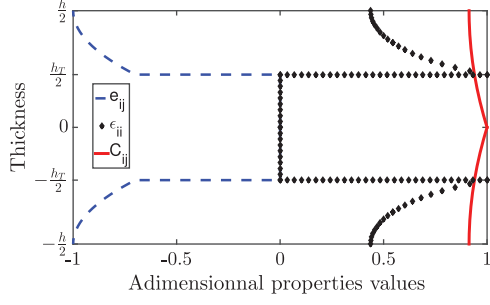


Figure 2. Effective properties through the thickness for $k = 2$ and $V_T = 30\%$.

2.2. FE formulation

The FE method is considered to analyse the FGPM plates. A triangular element is implemented from the FEniCS Project libraries (Logg et al., 2012). The formulation is based on first-order shear deformation theory (FSDT) hypothesis and on a layerwise approximation for electric potential. Numerical integration is performed taking into account the variation of the properties along the z direction.

2.2.1. Constitutive equations. The linear constitutive relations describing the electrical and mechanical interaction of piezoelectric material can be expressed as

$$\boldsymbol{\sigma} = \mathbf{C}\boldsymbol{\varepsilon} - \mathbf{e}\mathbf{E} \quad (8)$$

$$\mathbf{D} = \mathbf{e}\boldsymbol{\varepsilon} - \boldsymbol{\epsilon}\mathbf{E} \quad (9)$$

where $\boldsymbol{\sigma}$, $\boldsymbol{\varepsilon}$, \mathbf{D} and \mathbf{E} are the stress vector, the strain vector, the electrical displacement and the electric field, respectively. \mathbf{C} , \mathbf{e} and $\boldsymbol{\epsilon}$ are the elastic stiffness, piezoelectric and permittivity matrices, which are uniformly varying through the thickness.

In the case of plane stress condition ($\sigma_{33} = 0$), the constitutive equations become, using the Voigt notation

$$\begin{pmatrix} \sigma_1 \\ \sigma_2 \\ \sigma_4 \\ \sigma_5 \\ \sigma_6 \end{pmatrix} = \begin{bmatrix} \overline{C_{11}} & \overline{C_{12}} & 0 & 0 & 0 \\ \overline{C_{12}} & \overline{C_{22}} & 0 & 0 & 0 \\ 0 & 0 & \overline{C_{44}} & 0 & 0 \\ 0 & 0 & 0 & \overline{C_{55}} & 0 \\ 0 & 0 & 0 & 0 & \overline{C_{66}} \end{bmatrix} \begin{pmatrix} \varepsilon_1 \\ \varepsilon_2 \\ \varepsilon_4 \\ \varepsilon_5 \\ \varepsilon_6 \end{pmatrix} - \begin{bmatrix} 0 & 0 & \overline{e_{31}} \\ 0 & 0 & \overline{e_{32}} \\ 0 & \overline{e_{24}} & 0 \\ \overline{e_{15}} & 0 & 0 \\ 0 & 0 & 0 \end{bmatrix} \begin{pmatrix} E_1 \\ E_2 \\ E_3 \end{pmatrix} \quad (10)$$

$$\begin{pmatrix} D_1 \\ D_2 \\ D_3 \end{pmatrix} = \begin{bmatrix} 0 & 0 & 0 & \overline{e_{15}} & 0 \\ 0 & 0 & \overline{e_{24}} & 0 & 0 \\ \overline{e_{31}} & \overline{e_{32}} & 0 & 0 & 0 \end{bmatrix} \begin{pmatrix} \varepsilon_1 \\ \varepsilon_2 \\ \varepsilon_4 \\ \varepsilon_5 \\ \varepsilon_6 \end{pmatrix} + \begin{bmatrix} \overline{\epsilon_{11}} & 0 & 0 \\ 0 & \overline{\epsilon_{22}} & 0 \\ 0 & 0 & \overline{\epsilon_{33}} \end{bmatrix} \begin{pmatrix} E_1 \\ E_2 \\ E_3 \end{pmatrix} \quad (11)$$

with

$$\begin{cases} \overline{C_{pq}} = C_{pq} - \frac{C_{p3}C_{3q}}{C_{33}} \\ \overline{e_{ip}} = e_{ip} - \frac{e_{i3}C_{p3}}{C_{33}} \\ \overline{\epsilon_{ij}} = \epsilon_{ij} - \frac{C_{i3}C_{j3}}{C_{33}} \end{cases}$$

where subscripts (i,j) vary from 1 to 3 and subscripts (p,q) vary from 1 to 6.

2.2.2. Displacement approximation. The displacement field of an arbitrary point in the plate, based on the FSDT, can be expressed as

$$u_\alpha(x, y, z, t) = u_\alpha^0(x, y, t) + zu_\alpha^1(x, y, t) \quad (12)$$

$$u_3(x, y, z, t) = w(x, y, t) \quad (13)$$

with $\alpha = 1, 2$.

u_1 , u_2 and u_3 denote the displacements along the x -, y - and z -axes, respectively. u_1^0 , u_2^0 and w represent the displacements of the neutral surface, and u_1^1 and u_2^1 are the bending rotations. They are approximated using the Lagrange quadratic interpolation functions (Logg et al., 2012) and a six-node triangular element is considered, with 5 mechanical degrees of freedom per node.

2.2.3. Electric potential. As the FGPM is polarized in the z direction, the structure is discretized in n_l numerical layers in the thickness direction and a layerwise approximation is used (Polit and Bruant, 2006).

For a layer denoted (l) , and a reduced normal coordinate $\xi \in [-1, 1]$, the electric potential $\phi^{(l)}$ is approximated by Lagrange quadratic interpolation functions, using three potential values ($\phi_{bot}^{(l)}$, $\phi_{mid}^{(l)}$, $\phi_{top}^{(l)}$) located at the bottom, middle and top of this layer

$$\phi^{(l)}(x, y, z(\xi)) = h(\xi)\phi_{bot}^{(l)} + g(\xi)(1 - \xi^2)\phi_{mid}^{(l)} + f(\xi)\phi_{top}^{(l)} \quad (14)$$

with

$$f(\xi) = \frac{1}{2}\xi(\xi + 1) \quad g(\xi) = (1 - \xi^2) \quad h(\xi) = \frac{1}{2}\xi(\xi - 1) \quad (15)$$

For a layer with $z \in [z_{bot}^{(l)}, z_{top}^{(l)}]$, the relation between the thickness coordinate z and the reduce coordinate ξ is given by

$$z(\xi) = \frac{1}{2} \left(z_{top}^{(l)}(1 + \xi) + z_{bot}^{(l)}(1 - \xi) \right) \quad (16)$$

For the in-plane variation, a Lagrange linear approximation is considered. Therefore, a three-node triangular element is implemented to model the electric coupling, with $4n_l + 1$ electrical degrees of freedom per node.

2.2.4. The electro-mechanical system. Variational principles give the following discretized equations (Polit and Bruant, 2006)

$$\mathbf{K}_{uu}\mathbf{q} + \mathbf{M}_{uu}\ddot{\mathbf{q}} + \mathbf{K}_{u\phi}\phi = \mathbf{F} \quad (17)$$

$$\mathbf{K}_{\phi\phi}\phi + \mathbf{K}_{\phi u}\mathbf{q} = \mathbf{0} \quad (18)$$

where \mathbf{M}_{uu} is the global mass matrix, \mathbf{K}_{uu} is the global stiffness matrix, $\mathbf{K}_{u\phi}$ and $\mathbf{K}_{\phi u}$ are the global piezoelectric coupling stiffness matrices ($\mathbf{K}_{\phi u} = \mathbf{K}_{u\phi}^t$), $\mathbf{K}_{\phi\phi}$ is the global electric stiffness matrix, \mathbf{F} is the applied mechanical force vector, \mathbf{q} is the global nodal displacement vector and ϕ is the global element potential vector.

The potential can be split into two parts, the potentials of sensors and the ones of actuators, and using equation (18) in equation (17), we have the system (Benjeddou et al., 2006)

$$\mathbf{K}_{tot}\mathbf{q} + \mathbf{M}_{uu}\ddot{\mathbf{q}} = \mathbf{F} + \mathbf{K}_a\phi_a \quad (19)$$

$$\phi_s = -\mathbf{K}_{\phi_s\phi_s}^{-1}(\mathbf{K}_{\phi_s u}\mathbf{q} + \mathbf{K}_{\phi_s\phi_a}\phi_a) \quad (20)$$

where indexes s and a represent the sensors and actuators potentials, respectively, and

$$\mathbf{K}_{tot} = \mathbf{K}_{uu} + \mathbf{K}_{u\phi_s}\mathbf{K}_{\phi_s\phi_s}^{-1}\mathbf{K}_{\phi_s u} \quad (21)$$

$$\mathbf{K}_a = \mathbf{K}_{u\phi_s}\mathbf{K}_{\phi_s\phi_s}^{-1}\mathbf{K}_{\phi_s\phi_a} - \mathbf{K}_{u\phi_a} \quad (22)$$

2.2.5. The eigenvalues problem. The application of the active control methods in dynamic structural problems requires the use of state-space model. Thus, the normalized orthogonal structural modal basis Ψ must be considered. It is obtained from the following classical eigenvalues problem

$$(\mathbf{K}_{tot} - \omega^2\mathbf{M}_{uu})\Psi = \mathbf{0} \quad (23)$$

where ω and Ψ are the eigenfrequencies and the associated mode shapes, respectively.

3. Control system

In this section, the active control process is detailed. It is based on a state-space form model, a network of discrete electrodes used as actuators and sensors according to the most excited modes, and a fuzzy logic controller.

3.1. The modal analysis and the state-space form

To apply active vibration control to dynamic structural problems, the state-space form is useful (Burl, 1998). This form is based on the displacement's decomposition in the normalized orthogonal structural modal basis.

Assuming that contribution of the highest modes is negligible, only the N first modes are considered, and the displacement is approximated by

$$\mathbf{q} = \sum_{n=1}^N \Psi_n \alpha_n(t) = \Psi \boldsymbol{\alpha} \quad (24)$$

where Ψ_n is the n th mode and $\alpha_n(t)$ is the n th modal coordinate of the displacement \mathbf{q} .

Introducing equation (24) into equations (19) and (20) and using the orthogonality of eigenmodes yield to the state-space equations

$$\begin{cases} \dot{\mathbf{x}} = \mathbf{A}\mathbf{x} + \mathbf{B}\phi_a + \mathbf{f} \\ \mathbf{y} = \phi_s = \mathbf{C}\mathbf{x} \end{cases} \quad (25)$$

where \mathbf{x} is the state-space vector defined as

$$\mathbf{x} = \{\omega_1\alpha_1 \cdots \omega_N\alpha_N \quad \dot{\alpha}_1 \cdots \dot{\alpha}_N\}_{(2N,1)}^t \quad (26)$$

The state matrix \mathbf{A} , the control output matrix \mathbf{B} , the observation matrix \mathbf{C} and the load vector \mathbf{f} are defined as

$$\mathbf{A} = \begin{bmatrix} \mathbf{0} & \boldsymbol{\omega} \\ -\boldsymbol{\omega} & -2\boldsymbol{\eta}\boldsymbol{\omega} \end{bmatrix} \quad (27)$$

$$\mathbf{B} = \begin{bmatrix} \mathbf{0} \\ \Psi^t \mathbf{K}_a \end{bmatrix} \quad (28)$$

$$\mathbf{C} = \begin{bmatrix} \mathbf{K}_{\phi_s\phi_s}^{-1} \mathbf{K}_{\phi_s u} \Psi \boldsymbol{\omega}^{-1} & \mathbf{0} \end{bmatrix} \quad (29)$$

$$\mathbf{f} = \begin{Bmatrix} \mathbf{0} \\ \Psi^t \mathbf{F} \end{Bmatrix} \quad (30)$$

where $\boldsymbol{\omega}$ and $\boldsymbol{\eta}$ are the diagonal matrix containing the eigenfrequencies and the diagonal matrix of the natural damping ratio, respectively.

3.2. The active control process

The active control efficiency depends on several parameters: the location of actuators and sensors, the knowledge of the vibrations from the sensors output and the control law. As the FGPM concept allows us to put many electrodes on the top and bottom faces, which

can be used as actuators or sensors, an optimization procedure is considered to define the relevant actuators and sensors, based on controllability and observability criterias. Moreover, the devised smart FGPM must be well controlled for any excitation in a given frequency range: consequently, the fuzzy logic controller is used, as it is one of the most robust controllers.

3.2.1. Location of actuators and sensors. The location of actuators and sensors has a major influence on the performance of the control system. Wrong locations of sensors and actuators lead to problems such as the lack of observability or controllability. In this way, many studies have been published on this subject and different cost functions have been used to find the optimal locations of these active elements. In this article, the optimal location of sensors and actuators is considered independently. The modified optimization criteria developed in Bruant et al. (2010) are used. They ensure good observability and good controllability of each mode, enabling to consider all modes with homogeneity and not globally as it is usually done.

For the actuators location optimization, the usual objective is to find actuator locations that maximize a measure of the steady-state controllability Gramian matrix \mathbf{W}_c (Hać and Liu, 1993)

$$\mathbf{W}_c = \int_0^{\infty} \mathbf{e}^{\mathbf{A}t} \mathbf{B} \mathbf{B}^T \mathbf{e}^{\mathbf{A}^T t} dt \quad (31)$$

which tends to a diagonal form with

$$(W_c)_{nm} = (W_c)_{n+N, n+N} = \frac{1}{4\eta_n \omega_n} \sum_{j=1}^{N_a} B_{nj}^2 \quad (32)$$

$(W_c)_{nm}$ equals to the energy transmitted from the actuators to the structure for the n th eigenmode (Bruant and Proslie, 2005). If it is small, the n th eigenmode is difficult to control and there is no controllability for the system.

The usual criteria take into account globally the eigenmodes. To overcome this drawback, the considered optimization problem in Bruant and Proslie (2005) is to find the actuators location (a_1, \dots, a_{N_a}) which maximizes

$$J_A = \min_{n=1, N} \frac{(W_c(a_1, \dots, a_{N_a}))_{nm}}{\max_{a_1, \dots, a_{N_a}} (W_c(a_1, \dots, a_{N_a}))_{nm}} \quad (33)$$

The greatest advantage of this criterion is that all modes are studied with the same range and, for each mode, the values of the fraction inside equation (33) are in the interval $[0, 1]$. Furthermore, its expression has a physical meaning: it is the mechanical energy

transmitted for the n th mode divided by the maximal mechanical energy that could be received.

The optimal location of sensors is determined in the same way as the optimal location of actuators. It consists in maximizing the Gramian observability matrix defined by

$$\mathbf{W}_o = \int_0^{\infty} \mathbf{e}^{\mathbf{A}^T t} \mathbf{C}^T \mathbf{C} \mathbf{e}^{\mathbf{A} t} dt \quad (34)$$

which is diagonal dominant

$$(W_o)_{nm} = (W_o)_{n+N, n+N} = \frac{1}{4\eta_n \omega_n} \sum_{j=1}^{N_s} C_{jn}^2 \quad (35)$$

$$n = 1, \dots, N$$

To have a right information about the N first eigenmodes, and to insure homogeneity between each term $(W_o)_{ii}$, the optimization problem considered here is to find the sensors locations c_1, \dots, c_{N_s} which maximize

$$J_S = \min_{n=1, N} \frac{(W_o(c_1, \dots, c_{N_s}))_{nm}}{\max_{c_1, \dots, c_{N_s}} (W_o(c_1, \dots, c_{N_s}))_{nm}} \quad (36)$$

$\max_{c_1, \dots, c_{N_s}} (W_o(c_1, \dots, c_{N_s}))_{nm}$ represents the maximal output energy which could be measured for the n th mode by the sensors. The values of J_S are again in the interval $[0; 1]$.

3.2.2. The Luenberger observer. To implement a control law, the knowledge of the state vector \mathbf{x} (or the modal displacements and velocities) is necessary. This knowledge is not complete since only the output voltages \mathbf{y} are observed (equation (25)). Assuming that the state system verifies the observability criteria, at each time, an estimation $\hat{\mathbf{x}}$ is computed using a Luenberger observer (Kailath, 1980) according to

$$\dot{\hat{\mathbf{x}}} = \mathbf{A} \hat{\mathbf{x}} + \mathbf{B} \phi_{\alpha} + \mathbf{L}(\mathbf{y} - \mathbf{C} \hat{\mathbf{x}}) \quad (37)$$

where \mathbf{L} is the observance gain matrix. This matrix is chosen so that the real part of the eigenvalues of $\mathbf{A} - \mathbf{L} \mathbf{C}$ is negative.

3.2.3. Design of the fuzzy logic controller. The dynamic performance of smart structures depends on the control algorithm. There are numerous control algorithms which can be applied for active vibration with piezoelectric patches, such as direct proportional feedback, constant gain velocity feedback, constant amplitude velocity feedback, linear quadratic regulator (LQR) and H^2 control. These controls can be useful, but they are sensitive to structure characteristics. An alternative is the use of fuzzy logic control (FLC), where the control law is designed by human intelligence based on

expert's experience. This method is robust and can be applied for systems with uncertainties. It has been widely used in the past by a number of researchers for simulations of active vibration control of piezolaminated structures. Susheel et al. (2016) implemented this controller in the case of FGM plate with FGPM. Moreover, several experimental studies have been published to show the effectiveness of this controller like Gu and Song (2005), De Abreu and Ribeiro (2002), Li et al. (2011) and Lin (2005).

A conventional fuzzy controller follows three steps:

1. Fuzzification;
2. Rule base generation;
3. Defuzzification.

The fuzzification step performs the interpretation interface of input and output variables. Membership functions are used to transform input and output variables into linguistic control variables. The fuzzy relation between input and output variables is shown by fuzzy rules. They are derived from simple human reasoning and are based on the expert's experience. Most of authors use the Mamdani style inference which is in If-Then form (Mamdani, 1974). In the defuzzification step, the result of fuzzy inference is transformed into a numerical output value depending upon the rules. Usually, the centroid method is considered.

According to the authors, the use of fuzzy logic controller can be different from several main points:

- The equations of the model. The fuzzy logic controller can be computed from the FE equations (Kumar, 2013, Marinaki et al., 2015, Sharma et al., 2014, Susheel et al., 2016) or state/modal equations (De Abreu and Ribeiro, 2002; Li et al., 2011, Sharma et al., 2007; Zorić et al., 2013).
- The nature and the number of the membership functions. Most authors use triangular and trapezoidal functions for input and output variables: Sharma et al. (2007) and De Abreu and Ribeiro (2002) use three functions, Zorić et al. (2013) use five functions, Li et al. (2011), Lin (2005), Susheel et al. (2016) and Sharma et al. (2014) use seven functions, and Kumar (2013) uses nine functions. Marinaki et al. (2015) consider respectively three, five and nine triangular equations for velocity, displacement and control force. Gu and Song (2005) use Gaussian functions.
- How to apply the fuzzy controller method. Li et al. (2011) compute a decentralized adaptive fuzzy vibration controller, where each eigenmode is controlled by an actuator. In Sharma et al. (2007), an actuator is dedicated, at any time step, to control the mode that has the highest modal energy at this time. Lin (2005) applies a

decomposed parallel fuzzy control structure with one actuator. Each subsystem is associated with one mode and the total control action is the sum of each local control action.

In this work, the modal equations are considered and the active control is limited to the four first modes. A decentralized adaptive fuzzy controller is computed, considering actuators dedicated to each mode, from the optimization criteria (equation (33)). The electric potential applied is defined by a percentage of the mechanical modal energy at each time, in order to limit the used electrical energy, and to actuate the most relevant actuators according to the vibrations. Thus, for the controller dedicated to the i th mode, the inputs are the estimated modal displacement $\hat{\alpha}_i$ and modal velocity $\hat{\dot{\alpha}}_i$, and the output is the electric potential ϕ_a^i applied to the dedicated actuators. In order to have a simple controller, five triangular membership functions are considered for input and output variables, namely 'P+' (positive large), 'P' (positive), 'Z' (zero), 'N' (negative) and 'N+' (negative large). Zorić et al. (2013) has defined which shapes of triangular functions are efficient. They are plotted in Figure 3. As the inputs are set to be in $[-1, 1]$, at each time t , they are scaled, using a division by their maximal value, obtained in $[0, t]$

$$\bar{\alpha}_i(t) = \frac{\hat{\alpha}_i(t)}{\max_{\tau \in [0, t]} |\hat{\alpha}_i(\tau)|} \quad (38)$$

$$\bar{\dot{\alpha}}_i(t) = \frac{\hat{\dot{\alpha}}_i(t)}{\max_{\tau \in [0, t]} |\hat{\dot{\alpha}}_i(\tau)|} \quad (39)$$

The rules for active vibration control are given in Table 1. They are generated from Mamdani style inference. The centroid method is used for defuzzification and gives a value in $]-1, 1[$ for actuators voltage dedicated to the i th mode and named $\phi_c^i(t)$.

In order to damp best the most excited mode, without exceeding the admissible electric energy $J_i(t)$, defined as

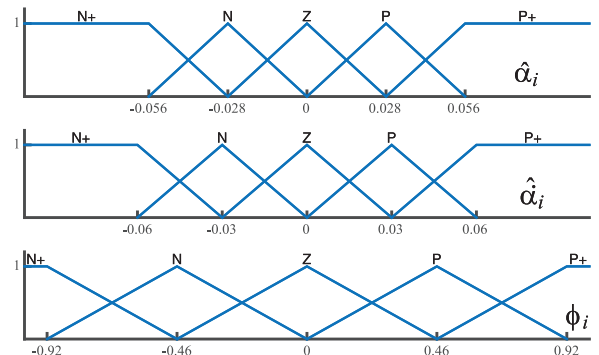


Figure 3. Triangular functions for fuzzy logic controller.

Table 1. Rule base for fuzzy logic controller.

$\bar{\alpha}_i$	$\bar{\alpha}_i$				
	N+	N	Z	P	P+
N+	P+	P+	P+	P	P
N	P	P	P	Z	Z
Z	P	P	Z	N	N
P	Z	Z	N	N	N
P+	N	N	N+	N+	N+

$$J_i(t) = \omega_i^2 \hat{\alpha}_i^2(t) + \hat{\alpha}_i^2(t) \quad (40)$$

and the weight of mechanical modal energy $W_i(t)$ as

$$W_i(t) = \frac{J_i(t)}{\sum_{i=1}^N J_i(t)} \quad \text{with } 0 \leq W_i(t) \leq 1 \quad (41)$$

In this way, the applied voltage devoted to the i th mode is given by

$$\phi_a^i(t) = \frac{\phi_c^i(t)}{\max|\phi_c^i|} \cdot V_{max} \cdot W_i(t) \quad (42)$$

where V_{max} represents the maximal admissible total voltage of the system and $\max|\phi_c^i|$ is the maximal value of ϕ_c^i compared to $\bar{\alpha}_i$ and $\bar{\alpha}_i$. Equation (42) leads to

$$0 \leq \sum_{i=1}^N \phi_a^i(t) \leq V_{max}$$

It allows to have a controller system, which activates with properly the suited actuators according to the most excited eigenmode, without exceeding the admissible electric energy.

4. Validation test

Before carrying out studies on active vibration control, the FE model has been validated with results of several papers for FGM. One test for FGPM is presented here, given by Zhong and Yu (2006).

We consider a single-layered FGPM square plate, simply supported and electrically grounded. The material properties vary in the direction of thickness as

$$P(z) = P^0 e^{\frac{z}{h}} \quad (43)$$

where $P = (C_{ij}, e_{ij}, \varepsilon_{ij}, \rho)$ and P^0 are the properties of PZT4, the reference material.

The first natural frequency is given in dimensionless form, $\bar{f}_1 = \omega_1 h / 2\pi \sqrt{\rho / C_{11}}$, where ω is the natural frequency, C_{11} an elastic coefficient and ρ the mass density.

The first natural frequencies for a thickness ratio $h/L = 0.1$ and for different values of k are given in

Table 2. Comparison of the first dimensionless frequency of a FGPM square plate by Zhong and Yu (2006).

k	0	0.1	1	2	5
$\bar{f}_1 \times 10^{-3}$ (Zhong)	8.14	8.14	7.85	7.14	4.87
$\bar{f}_1 \times 10^{-3}$ (Present)	8.32	8.32	7.97	7.30	4.92

Table 2. The results are compared to the exact solution given by Zhong and Yu (2006). The FE gives excellent results as the error is less than 3%.

5. Active control simulations

In this section, a $1.0 \text{ m} \times 0.8 \text{ m} \times 0.01 \text{ m}$ rectangular simply supported FGPM plate, made from a mixture of PZT4 and aluminium, with a percolation threshold equal to $V_T = 30\%$, is considered. The mechanical and electrical properties of these two materials are given in Table 3. As presented in Figure 4, 16 electrodes ($0.1 \text{ m} \times 0.06 \text{ m}$) are printed on the top and bottom faces of the plate, allowing 16 possible locations for sensors pairs and actuators pairs (upper and lower parts of the active areas are simultaneously used as sensors or actuators).

The aim of the present simulation is to control the first four eigenmodes (bending ones). Nevertheless, the first six eigenfrequencies, detailed in Table 4 in the case of $k = 2$, are taken into account to build the controllers in order to avoid spillover. The natural damping of the plate will be taken into account through the damping ratio given by the Rayleigh relation (Clough and Penzien, 1975)

Table 3. Characteristics of PZT4 and aluminium.

Properties	Aluminium	PZT4
Young modulus Y (GPa)	69	–
Poisson ratio ν	0.3	–
Piezoelectric constants (C/m ²)		
$e_{31} = e_{32}$	–	–5.2
$e_{15} = e_{24}$	–	2.7
e_{33}	–	15.1
Dielectric constants (nF/m)		
$\epsilon_{11} = \epsilon_{22}$	–	13.09
ϵ_{33}	26.55e ⁻³	11.51
Elastic constant (GPa)		
$C_{11} = C_{22}$	–	139
C_{33}	–	115
C_{12}	–	77.8
C_{13}	–	74.3
$C_{44} = C_{55}$	–	25.6
C_{66}	–	30.6
Density ρ (kg/m ³)	3960	7600

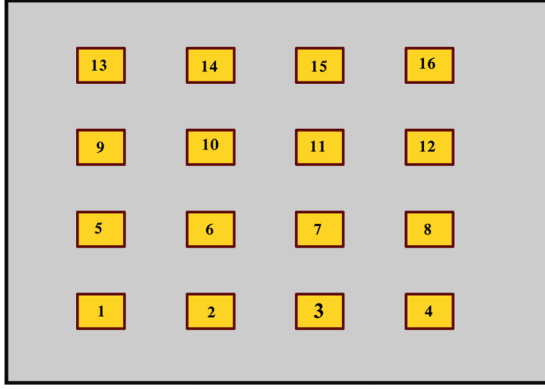


Figure 4. Electrodes locations on the FGPM plate.

Table 4. Eigenfrequencies for $k = 2$ (Hz).

f_1	f_2	f_3	f_4	f_5	f_6
38.78	84.38	110.33	155.98	160.67	229.49

Table 5. Actuators dedicated to each eigenmode.

Eigenmode	1	2	3	4
Actuators electrodes	6, 11	5, 8	2, 14	1, 16

$$\eta_i = \frac{\gamma\omega_i}{2} + \frac{\beta}{2\omega_i}$$

where γ and β are constants equal to

$$\gamma = \frac{0.004}{(\omega_1 + \omega_2)}, \quad \beta = \gamma\omega_1\omega_2$$

As the structure has two normal symmetric planes to the neutral surface, each eigenmode is controlled by a set of two actuator pairs, each electrode receiving the same electric potential. The modified optimization criteria (equation (33)) is used to define which electrodes are well suited to control each eigenmode. Results are given in Table 5. Similarly, using criteria (equation (36)), electrodes 3 and 9 are considered as sensors.

In the following simulations, the plate is subjected to a release test ($x_i(t=0) = 10^{-4}$ m for $i = 1, 2, 3, 4$) and a uniform load (10^3 Pa) is applied at $t = 1$ s during 0.11 s such as to model a mechanical impact. Finally, at each time, the maximal value of the total electric potential applied to the electrodes is $V_{max} = 250$ V.

5.1. Results for a classical fuzzy controller

In this first simulation, a classical fuzzy controller (CFC) is considered. It consists in a control of each eigenmode, independently of each other. The input of each pair of actuators is obtained by a fuzzy controller and is limited to the value of 62.5 V, in order not to exceed the V_{max} threshold.

The open-loop time response (uncontrolled plate) of the four first modal coordinates is presented in Figure 5. The magnitude decay here observed comes from the natural damping of the plate.

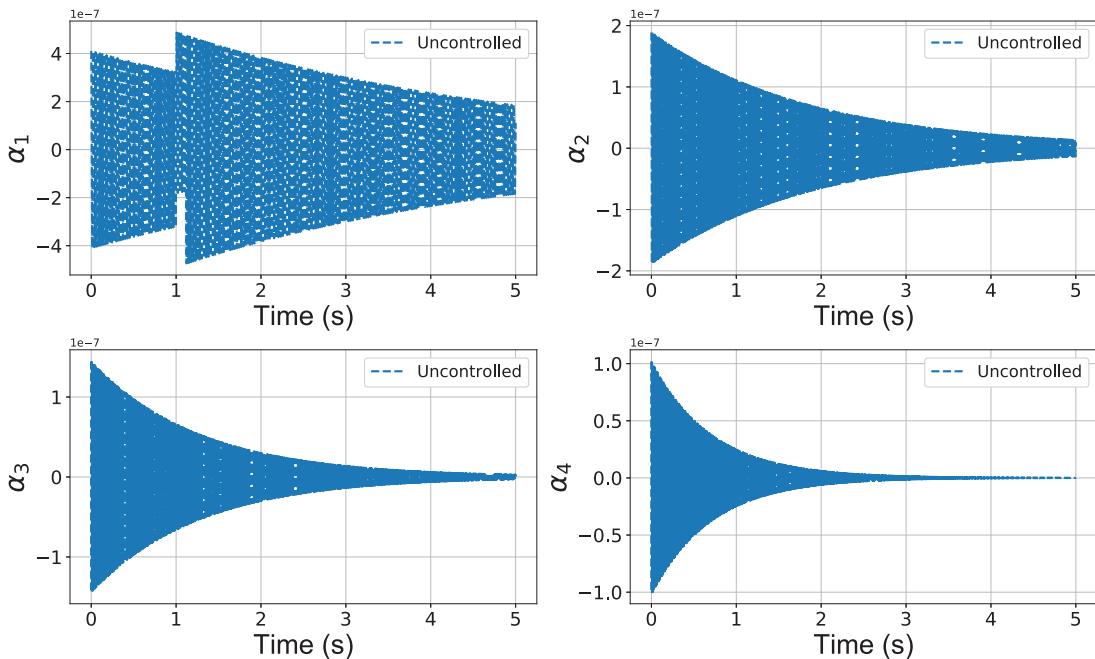


Figure 5. The first four modal coordinates in the case of open loop.

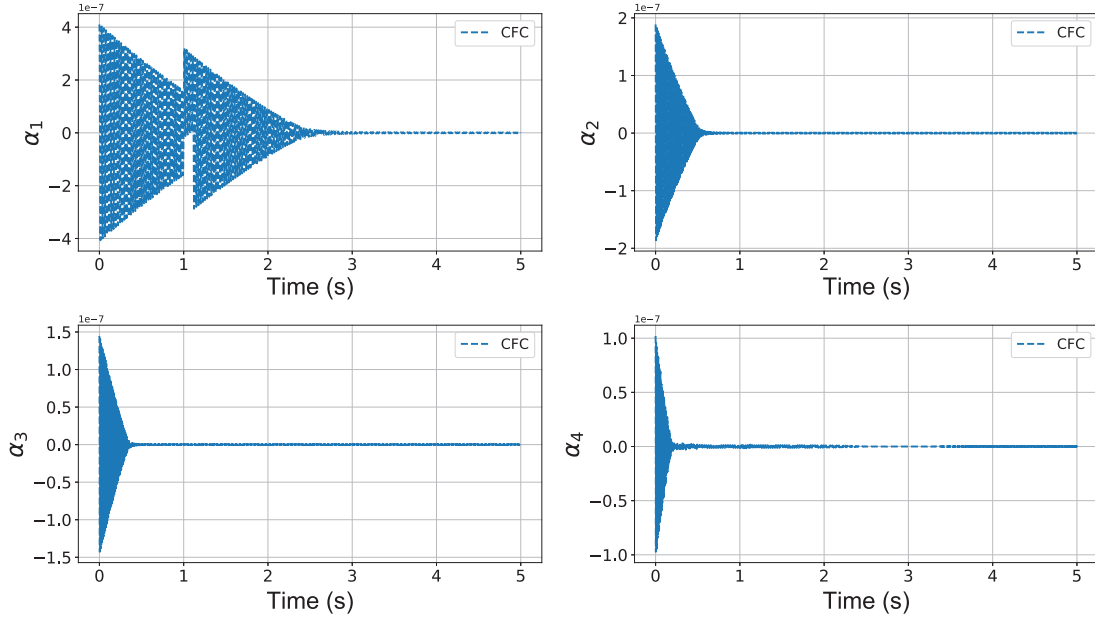


Figure 6. The first four modal coordinates in the case of closed loop, using a classical fuzzy controller.

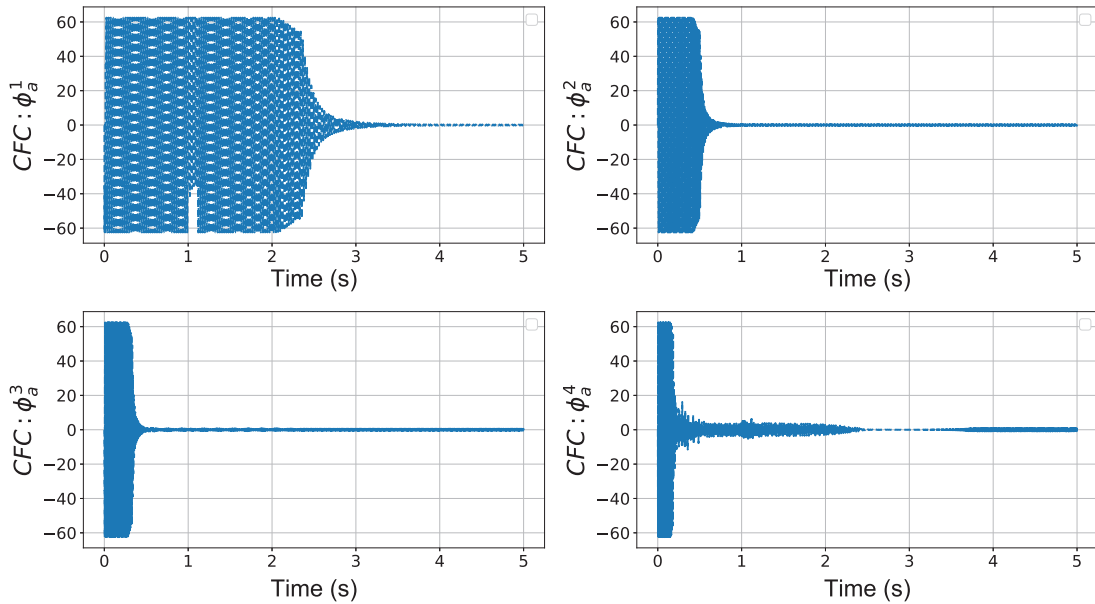


Figure 7. The actuator inputs from a classical fuzzy controller.

Figures 6 and 7 respectively present the closed-loop time response (controlled plate) and the potential applied to the four pairs of actuators electrodes.

It can be noted that the vibrations of eigenmodes 2, 3 and 4 vanish in less than 0.5 s. On the other hand, the greater mechanical energy needed to control the first mode and the limited potential on electrodes led to an extended control time (about 3 s).

5.2. Results for adaptive fuzzy controller

In this section, the adaptive fuzzy controller (AFC) is used, taking into account the most excited eigenmodes. The electric potentials applied to each actuator pair are now given by equation (42). They depend on the mechanical modal energy percentage of each mode in order to ensure that the most electrical energy is applied to control the most excited modes.

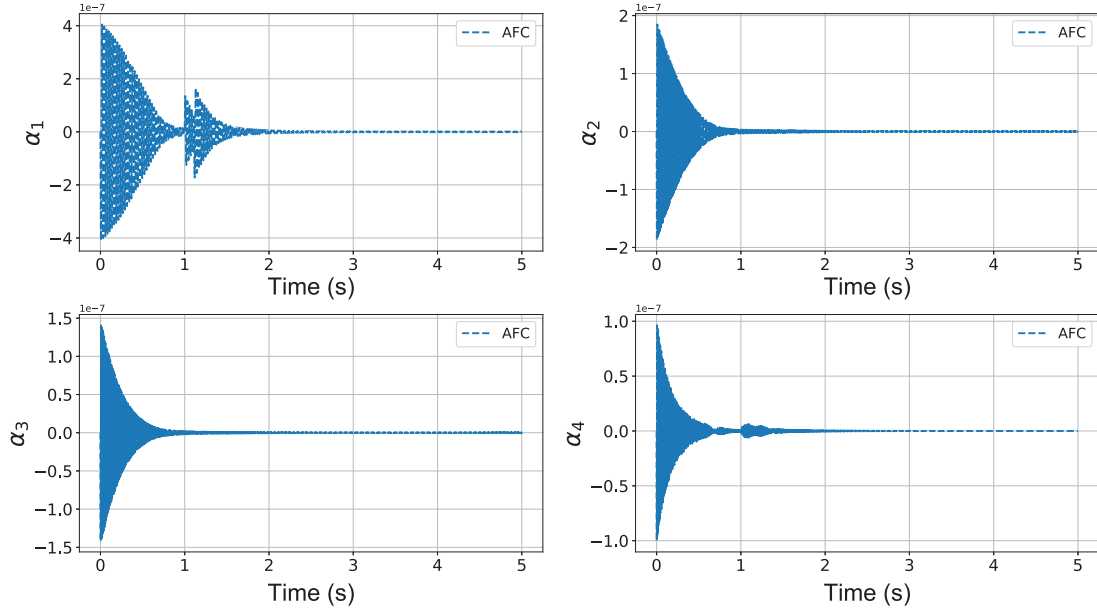


Figure 8. The first four modal coordinates in the case of closed loop, using the adaptive fuzzy controller.

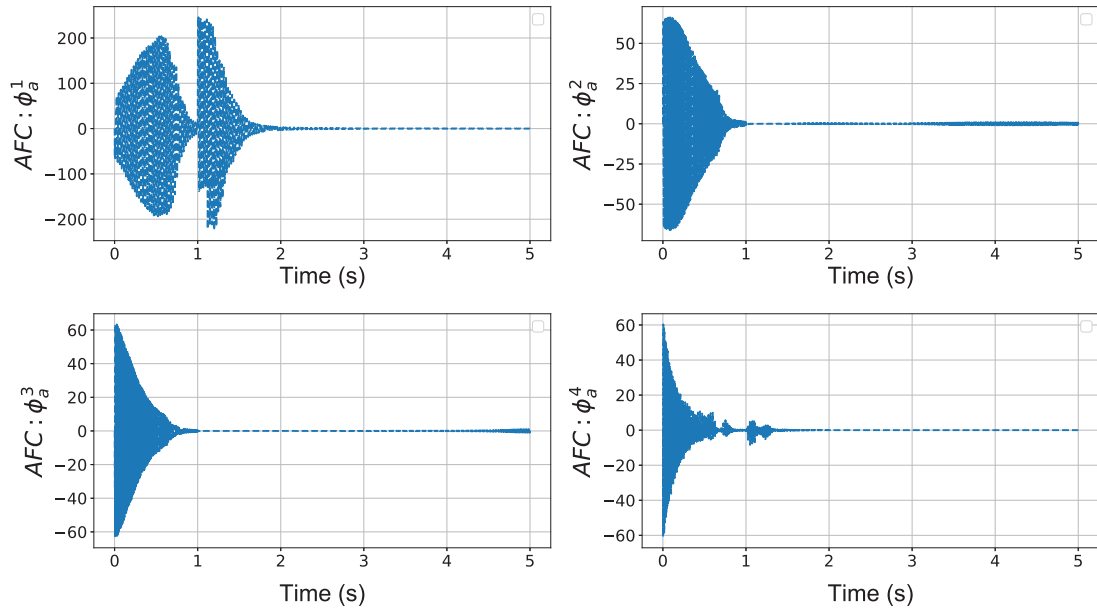


Figure 9. The actuator inputs from the adaptive fuzzy controller.

The four modal coordinates and the actuators inputs are plotted in Figures 8 and 9. The first mode being the most excited one, the input of actuators for mode 1 is higher than those for modes 2 to 4. As a consequence, the controller efficiency increases for the first mode: the release load nearly vanishes before the impact load and both of them are controlled in less than 2 s. On the other hand, the time needed to control modes 2 to 4 are increased weakly, but all modes are controlled in less than 2 s.

In Figure 10, the deflection of the FGPM at the location (0.5 m, 0.4 m) is plotted for the uncontrolled

system and the two fuzzy controllers. It can be noted that the AFC allows vibrations to vanish more than twice as fast as the CFC.

5.3. Comparison with the LQR

The LQR is one of the most usual control method used in active vibration control of classical structures (Bruant and Proslie, 2015; Preumont, 2011). In Balamurugan and Narayanan (2001), several control laws are compared for active control of plates, and the LQR optimal control schemes are proved to be more

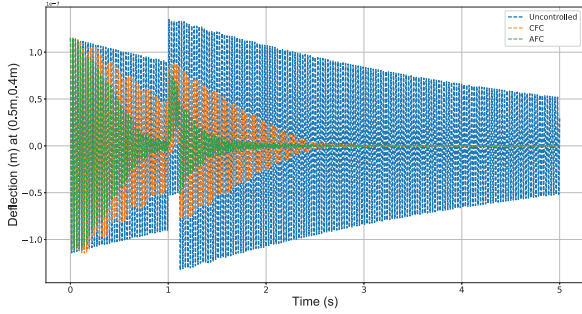


Figure 10. The deflection of the FGPM plate, at the location (0.5 m, 0.4 m).

effective than classical controls. However, this method is useful in using one or two actuators but its implementation becomes complicated for more than two devices. In this section, a comparison between AFC (using four pairs of actuators) with LQR (using one actuator located at location 6, the optimal location for the fourth modes) is presented. Similarly to previous simulations, the maximal value of the total electric potential is still $V_{max} = 250$ V.

Assuming that the state equation is controllable, the control law may be written as Kailath (1980)

$$\phi_a = -\mathbf{K}\mathbf{x} \quad (44)$$

which minimizes a cost function given by

$$J_\phi = \frac{1}{2} \int_0^\infty (\mathbf{x}^T \mathbf{Q} \mathbf{x} + \phi_a^T \mathbf{R} \phi_a) dt \quad (45)$$

\mathbf{R} is a positive matrix and \mathbf{Q} is a positive semi-definite matrix. The optimal solution is

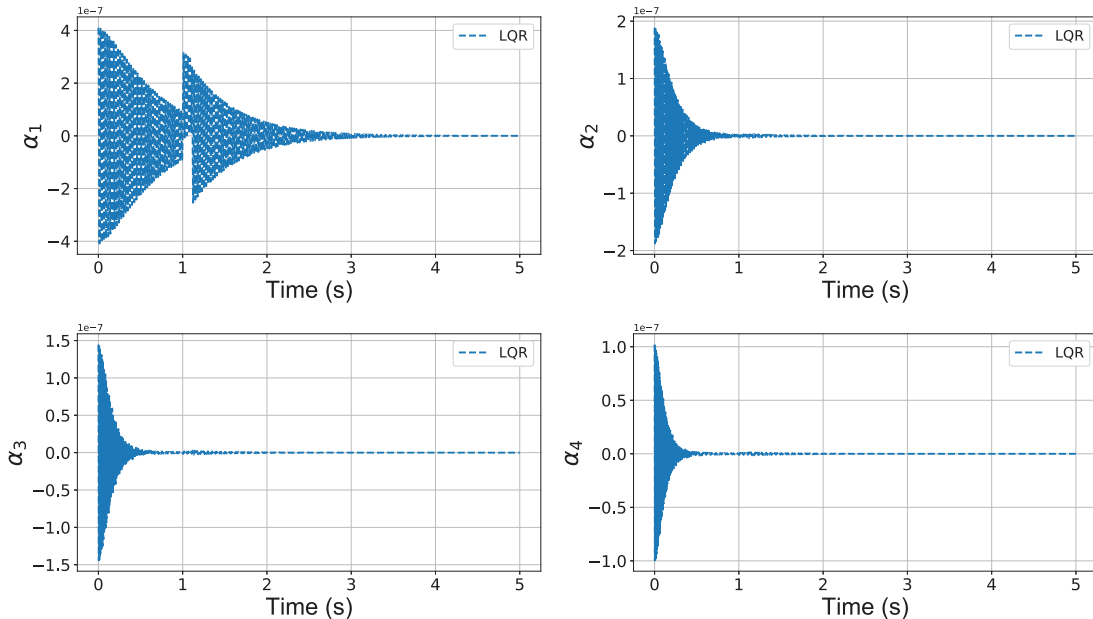


Figure 11. The first four modal coordinates in the case of closed loop, using the LQR controller.

$$\mathbf{K} = \mathbf{R}^{-1} \mathbf{B}^T \mathbf{P} \quad (46)$$

where \mathbf{P} satisfies the Riccati equation

$$\mathbf{A}^T \mathbf{P} + \mathbf{P} \mathbf{A} - \mathbf{P} \mathbf{B} \mathbf{R}^{-1} \mathbf{B}^T \mathbf{P} + \mathbf{Q} = \mathbf{0} \quad (47)$$

In the following application, \mathbf{Q} is chosen so that $\mathbf{x}^T \mathbf{Q} \mathbf{x}$ represents the mechanical energy. The components of \mathbf{R} are chosen using the following statement: the maximal values of ϕ_a are less than V_{max} . As the knowledge of \mathbf{x} is usually not complete, the control law uses $\hat{\mathbf{x}}$, the estimation of \mathbf{x}

$$\phi_a = -\mathbf{K} \hat{\mathbf{x}} \quad (48)$$

where $\hat{\mathbf{x}}$ is an estimation of \mathbf{x} .

Figures 11 to 13 respectively present the time response, the potential applied to the actuator and the tip deflection at the location (0.5 m, 0.4 m) for the LQR controller.

The efficiency of the LQR controller is quite good for the release test. Nevertheless, the matrix \mathbf{K} of the LQR controller being optimized for one defined disturbance (here the release test), this controller is less efficient than the AFC controller for the applied uniform load at time $t = 1$ s. On the other hand, the fuzzy methods are known to be well suited for uncertainties, especially for disturbance uncertainties.

6. Conclusion

Active vibration control of a smart FGPM plate has been carried out using an adaptive fuzzy controller strategy. The mechanical and electrical properties of the FGPM are graded in the thickness according to a power law distribution, with the exception of the

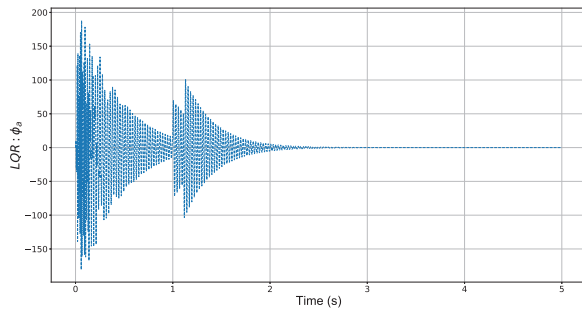


Figure 12. The actuator input from the LQR controller.

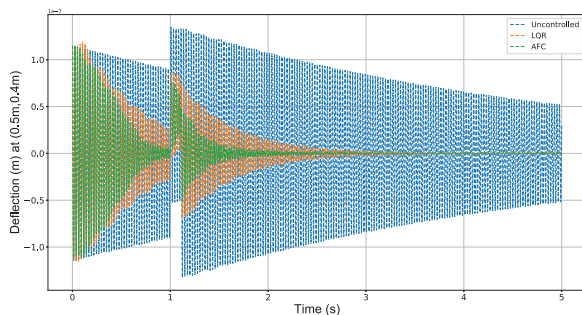


Figure 13. The deflection of the FGPM plate, at the location (0.5 m, 0.4 m).

permittivity, which follows the Maxwell-Garnett Law. Insulating and conductive regions in the FGPM are derived from the percolation phenomenon. In this work, the FGPM is considered symmetrically distributed, without imperfection.

A FGPM plate FE based on the FSDT hypothesis and layerwise approximation for electric potential has been implemented to obtain the modal basis used for active control. The FGPM being equipped with a network of discrete electrodes, an optimization procedure has been used to define the relevant electrodes for actuators and sensors, based on controllable and observable criteria. An AFC system has been used, activating with relevance the actuators according to the most excited eigenmodes. Simulations show the effectiveness of this kind of concept and fuzzy controller.

This article is a first study showing the feasibility of active vibration control using such materials. The study of uncertainty in this distribution will be an upcoming work.

Declaration of conflicting interests

The author(s) declared no potential conflicts of interest with respect to the research, authorship and/or publication of this article.

Funding

The author(s) received no financial support for the research, authorship and/or publication of this article.

ORCID iD

Isabelle Bruant  <https://orcid.org/0000-0003-0837-3410>

References

- Balamurugan V and Narayanan S (2001) Shell finite element for smart piezoelectric composite plate/shell structures and its application to the study of active vibration control. *Finite Elements in Analysis and Design* 37(9): 713–738.
- Barati MR and Zenkour AM (2018) Electro-thermoelastic vibration of plates made of porous functionally graded piezoelectric materials under various boundary conditions. *Journal of Vibration and Control* 24(10): 1910–1926.
- Behjat B, Salehi M, Armin A, et al. (2011) Static and dynamic analysis of functionally graded piezoelectric plates under mechanical and electrical loading. *Scientia Iranica* 18(4): 986–994.
- Benjeddou A, Belouettar S, Topping B, et al. (2006) On the evaluation and application of the modal properties of piezoelectric adaptive structures. In: Topping BHV, Montero G and Montenegro R (eds) *Innovation in Computational Structures Technology*. Stirling: Saxe-Coburg Publications, pp. 287–302.
- Bodaghi M, Damanpack A, Aghdam M, et al. (2012) Non-linear active control of FG beams in thermal environments subjected to blast loads with integrated FGP sensor/actuator layers. *Composite Structures* 94(12): 3612–3623.
- Brischetto S and Carrera E (2009) Refined 2D models for the analysis of functionally graded piezoelectric plates. *Journal of Intelligent Material Systems and Structures* 20(15): 1783–1797.
- Bruant I and Proslie L (2005) Optimal location of actuators and sensors in active vibration control. *Journal of Intelligent Material Systems and Structures* 16(3): 197–206.
- Bruant I and Proslie L (2015) Improved active control of a functionally graded material beam with piezoelectric patches. *Journal of Vibration and Control* 21(10): 2059–2080.
- Bruant I, Gallimard L and Nikoukar S (2010) Optimal piezoelectric actuator and sensor location for active vibration control, using genetic algorithm. *Journal of Sound and Vibration* 329(10): 1615–1635.
- Burl JB (1998) *Linear Optimal Control: H_2 and H_∞ (Infinity) Methods*. Boston, MA: Addison-Wesley.
- Chýlek P and Srivastava V (1983) Dielectric constant of a composite inhomogeneous medium. *Physical Review B* 27(8): 5098.
- Clough RW and Penzien Y (1975) *Dynamiques des Structures*. New York: McGraw-Hill.
- De Abreu GLC and Ribeiro JF (2002) A self-organizing fuzzy logic controller for the active control of flexible structures using piezoelectric actuators. *Applied Soft Computing* 1(4): 271–283.
- Doroushi A, Eslami M and Komeili A (2011) Vibration analysis and transient response of an FGPM beam under thermo-electro-mechanical loads using higher-order shear deformation theory. *Journal of Intelligent Material Systems and Structures* 22(3): 231–243.
- Fakhari V and Ohadi A (2011) Nonlinear vibration control of functionally graded plate with piezoelectric layers in thermal environment. *Journal of Vibration and Control* 17(3): 449–469.

- Gu H and Song G (2005) Active vibration suppression of a composite I-beam using fuzzy positive position control. *Smart Materials and Structures* 14(4): 540.
- Hać A and Liu L (1993) Sensor and actuator location in motion control of flexible structures. *Journal of Sound and Vibration* 167(2): 239–261.
- He X, Ng T, Sivashanker S, et al. (2001) Active control of FGM plates with integrated piezoelectric sensors and actuators. *International Journal of Solids and Structures* 38(9): 1641–1655.
- Kailath T (1980) *Linear Systems*, vol. 156. Englewood Cliffs, NJ: Prentice-Hall.
- Kiani Y, Sadighi M and Eslami M (2013) Dynamic analysis and active control of smart doubly curved FGM panels. *Composite Structures* 102: 205–216.
- Kumar V (2013) Vibration control of a plate with help of fuzzy logic controller. *International Journal of Enhanced Research in Science Technology and Engineering* 2: 100–106.
- Li D, Liu W, Jiang J, et al. (2011) Placement optimization of actuator and sensor and decentralized adaptive fuzzy vibration control for large space intelligent truss structure. *Science China Technological Sciences* 54(4): 853–861.
- Li JF, Takagi K, Terakubo N, et al. (2001) Electrical and mechanical properties of piezoelectric ceramic/metal composites in the Pb(Zr, Ti)O₃/Pt system. *Applied Physics Letters* 79(15): 2441–2443.
- Liew K, Sivashanker S, He X, et al. (2003) The modelling and design of smart structures using functionally graded materials and piezoelectrical sensor/actuator patches. *Smart Materials and Structures* 12(4): 647–655.
- Lin J (2005) An active vibration absorber of smart panel by using a decomposed parallel fuzzy control structure. *Engineering Applications of Artificial Intelligence* 18(8): 985–998.
- Logg A, Mardal KA and Wells G (2012) *Automated Solution of Differential Equations by the Finite Element Method: The Fenics Book*, vol. 84. Berlin: Springer Science + Business Media.
- Mahamood RM, Akinlabi ET, Shukla M, et al. (2012) Functionally graded material: an overview. In: *Proceedings of the world congress on engineering (WCE)*, London, 4–6 July.
- Mamdani EH (1974) Application of fuzzy algorithms for control of simple dynamic plant. In: *Proceedings of the Institution of Electrical Engineers* 121: 1585–1588.
- Marinaki M, Marinakis Y and Stavroulakis GE (2015) Fuzzy control optimized by a multi-objective differential evolution algorithm for vibration suppression of smart structures. *Computers & Structures* 147: 126–137.
- Maruani J, Bruant I, Pablo F, et al. (2017) A numerical efficiency study on the active vibration control for a FGPM beam. *Composite Structures* 182: 478–486.
- Narayanan SBV (2010) Functionally graded shells with distributed piezoelectric sensors and actuators for active vibration control. In: Dattaguru B, Gopalakrishnan S and Aatre V (eds) *IUTAM Symposium on Multi-Functional Material Structures and Systems*, vol. 19. Dordrecht: Springer, pp. 3–13.
- Nourmohammadi H and Behjat B (2016) Design criteria for functionally graded piezoelectric plates under thermo-electro-mechanical loadings. *Journal of Intelligent Material Systems and Structures* 27(16): 2249–2260.
- Orlowska S (2003) *Conception et prédiction des caractéristiques diélectriques des matériaux composites à deux et trois phases par la modélisation et la validation expérimentale*. PhD Thesis, Ecole Centrale de Lyon, Écully.
- Pecharromán C and Moya JS (2000) Experimental evidence of a giant capacitance in insulator–conductor composites at the percolation threshold. *Advanced Materials* 12(4): 294–297.
- Polit O and Bruant I (2006) Electric potential approximations for an eight node plate finite element. *Computers & Structures* 84(22): 1480–1493.
- Preumont A (2011) *Vibration Control of Active Structures: An Introduction*, vol. 179. Berlin: Springer Science + Business Media.
- Pritchard J, Bowen C and Lowrie F (2013) Multilayer actuators: review. *British Ceramic Transactions* 100(6): 265–273.
- Sharma A, Kumar A, Kumar R, et al. (2016) Finite element analysis on active vibration control using lead zirconate titanate–Pt-based functionally graded piezoelectric material. *Journal of Intelligent Material Systems and Structures* 27(4): 490–499.
- Sharma A, Kumar R, Vaish R, et al. (2014) Lead-free piezoelectric materials’ performance in structural active vibration control. *Journal of Intelligent Material Systems and Structures* 25(13): 1596–1604.
- Sharma M, Singh S and Sachdeva B (2007) Modal control of a plate using a fuzzy logic controller. *Smart Materials and Structures* 16(4): 1331.
- Sheng G and Wang X (2009) Active control of functionally graded laminated cylindrical shells. *Composite Structures* 90(4): 448–457.
- Susheel C, Kumar R and Chauhan VS (2016) Active shape and vibration control of functionally graded thin plate using functionally graded piezoelectric material. *Journal of Intelligent Material Systems and Structures* 28(13): 1789–1802.
- Takagi K, Li JF, Yokoyama S, et al. (2002) Design and fabrication of functionally graded PZT/Pt piezoelectric bimorph actuator. *Science and Technology of Advanced Materials* 3(2): 217–224.
- Yiqi M and Yiming F (2010) Nonlinear dynamic response and active vibration control for piezoelectric functionally graded plate. *Journal of Sound and Vibration* 329(11): 2015–2028.
- Zheng S, Dai F and Song Z (2009) Active control of piezothermoelastic FGM shells using integrated piezoelectric sensor/actuator layers. *International Journal of Applied Electromagnetics and Mechanics* 30(12): 107–124.
- Zhong Z and Yu T (2006) Vibration of a simply supported functionally graded piezoelectric rectangular plate. *Smart Materials and Structures* 15(5): 1404.
- Zorić N, Simonović A, Mitrović Z, et al. (2013) Active vibration control of smart composite beams using PSO-optimized self-tuning fuzzy logic controller. *Journal of Theoretical and Applied Mechanics* 51(2): 275–286.